Ultrasonics Sonochemistry 31 (2016) 355–361

Contents lists available at ScienceDirect

Ultrasonics Sonochemistry

journal homepage: www.elsevier.com/locate/ultson

Synchrotron quantification of ultrasound cavitation and bubble dynamics in Al–10Cu melts

W.W. Xu [a,b], I. Tzanakis [c,1], P. Srirangam [d], W.U. Mirihanage [a,b,*], D.G. Eskin [c], A.J. Bodey [e], P.D. Lee [a,b]

[a] Manchester X-ray Imaging Facility, University of Manchester, Manchester M13 9PL, UK
[b] Research Complex at Harwell, Didcot OX11 0FA, UK
[c] Brunel Centre for Advanced Solidification Technology, Brunel University London, Uxbridge UB8 3PH, UK
[d] WMG, University of Warwick, Coventry CV4 7AL, UK
[e] Diamond Light Source Ltd, Didcot OX11 0DE, UK

ARTICLE INFO

Article history:
Received 15 October 2015
Received in revised form 18 December 2015
Accepted 15 January 2016
Available online 18 January 2016

Keywords:
Synchrotron X-ray radiography
Ultrasound cavitation
Cavitation bubble
Degassing
Al–Cu alloy

ABSTRACT

Knowledge of the kinetics of gas bubble formation and evolution under cavitation conditions in molten alloys is important for the control casting defects such as porosity and dissolved hydrogen. Using *in situ* synchrotron X-ray radiography, we studied the dynamic behaviour of ultrasonic cavitation gas bubbles in a molten Al–10 wt% Cu alloy. The size distribution, average radius and growth rate of cavitation gas bubbles were quantified under an acoustic intensity of 800 W/cm^2 and a maximum acoustic pressure of 4.5 MPa (45 atm). Bubbles exhibited a log-normal size distribution with an average radius of 15.3 ± 0.5 μm. Under applied sonication conditions the growth rate of bubble radius, $R(t)$, followed a power law with a form of $R(t) = \alpha t^{\beta}$, and $\alpha = 0.0021$ & $\beta = 0.89$. The observed tendencies were discussed in relation to bubble growth mechanisms of Al alloy melts.

1. Introduction

Liquid metal engineering, including the application of external physical fields, is regarded as an important approach for the control of microstructure and the resulting mechanical properties of many metallic materials [1–3]. Ultrasonic treatment has been employed in solidification processing to achieve structure control [4], grain refinement [5] and degassing [6]. Particularly, its application to light metal (Al and Mg-based) alloys has attracted great interest recently [7]. The mechanisms of ultrasonic treatment include formation, oscillation and collapse of cavitation bubbles; thus promoting melt degassing, wetting and dispersion of solidification phases, including refinement of primary intermetallics and dendrite fragmentation [5–8]. Understanding of ultrasonic cavitation mechanisms and cavitation bubbles through experimental investigation can significantly contribute to reducing casting defects such as porosity through effective control of the dissolved hydrogen content [6]. In addition, such studies can provide insights on other cavitation-related phenomena such as fragmentation and deagglomeration [8–10], and for the validation of numerical models [9,10].

With conventional characterisation techniques, it has been difficult to directly observe ultrasonic cavitation in molten metals due to their opaqueness and high temperature. In recent years, synchrotron X-ray imaging has been extensively applied to the *in situ* study of solidification [2,11,12], fragmentation [8,13] and coarsening mechanisms [14], pore and bubble growth during solidification [15,16], and semi-solid processing [17–19]. Huang et al. [20] recently reported measurement of the size distribution of cavitation gas bubbles in an Al–Cu alloy melt using the synchrotron X-ray radiography whilst the current authors used it to study the ultrasonic capillary effect in a molten metallic alloy [21]. Tan et al. [22] observed shockwaves and flows upon cavitation in Bi-based alloys. However, the growth behaviour, number density and underlying mechanisms of cavitation bubble have not been investigated.

In this article we report an *in situ* synchrotron X-ray radiography experiment in which we observed cavitation bubbles induced by an external ultrasound field in a molten Al–10 wt% Cu alloy. Collected statistical data of cavitation bubbles was used to analyse their size distribution and dynamics. The results are discussed in relation to ultrasonic melt degassing.

* Corresponding author at: Manchester X-ray Imaging Facility – Research Complex at Harwell, Rutherford Appleton Laboratory, Didcot OX11 0FA, UK. Fax: +441235567497.

[1] Faculty of Technology, Design and Environment, Oxford Brookes University, Wheatley OX33 1HX, UK.

http://dx.doi.org/10.1016/j.ultsonch.2016.01.017
1350-4177/

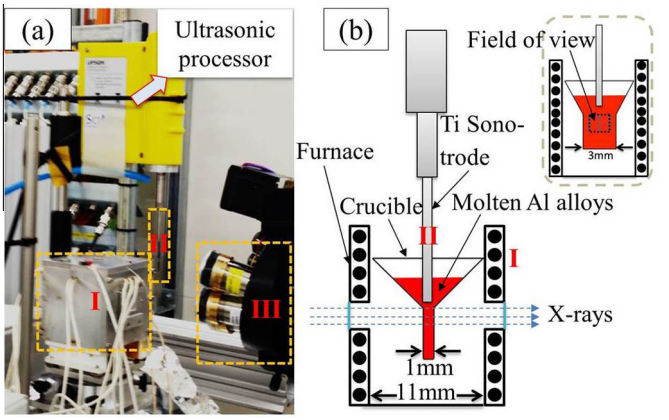

Fig. 1. (a) *In situ* ultrasonic processing setup on Diamond-Manchester branchline. (b) Schematic diagram of the furnace and crucible (inset is the view along X-ray beam). Main components: (I) – furnace; (II) – Ti sonotrode integrated with the ultrasonic processor; (III) – camera.

2. Methods

2.1. Experiments

In situ synchrotron X-ray radiography was conducted at the I13-2 Diamond-Manchester Imaging Branchline of Diamond Light Source, UK. The experimental setup is shown in Fig. 1(a) with key dimensions of the boron nitride (BN) crucible and furnace shown in Fig. 1(b). A bespoke PID-controlled resistance furnace ('Etna') [17] equipped with an X-ray translucent window, was integrated into the beamline to melt and contain the samples. Al–10 wt% Cu alloy samples were pre-machined in order to fit the cavity of the crucible and both were placed at the centre of the furnace cavity.

The crucible was machined from BN due to the material's low X-ray attenuation relative to the Al–Cu alloy. Its cavity was 1.00 ± 0.05 mm wide (in the direction of beam propagation), which provided reasonable imaging capability under the filtered pink beam (mode energy ~15 keV). The alloy was melted and stabilized at 660 ± 10 °C (~30 °C above the liquidus). Subsequently, a Ti sonotrode with a 1 mm diameter tip, mounted on an ultrasonic processor operating at 30 kHz (Hielscher, Germany), was immersed to a depth of ~4 mm in the melt. The ultrasonic processor was used to generate longitudinal mechanical vibrations by means of electric excitation (reverse piezoelectric effect). A $CdWO_4$ scintillator-coupled pco.edge 5.5 (PCO AG, Germany) camera along with ×10 optical magnification module provided a field of view of 2.1 × 1.8 mm and an effective pixel size of 0.81 μm. The camera operated at 13 frames per second (fps) with an exposure time of 25 ms. The centre of the viewing window was then positioned at an approximate distance of 5.00 mm below the sonotrode tip during ultrasonication. The ultrasonic processing parameters used in this work are summarised in Table I. As a result, an output pressure of 4.5 MPa is effectively generated on the tip of the sonotrode in the melt, calculated using the analytical model in [23].

Table I
Conditions of external ultrasound field imposed onto alloy melt.

Parameters	Working specification
Driving frequency	30 kHz
Amplitude (peak-to-peak)	28 μm
Pulse–pulse mode factor	50% per second (i.e. one cycle duration: 1 s)
Acoustic power density	800 W/cm^2
Processing time	44 s (i.e. 44 cycles)

2.2. Image analysis

Cavitation bubbles were usually found to be approximately spherical, i.e., circular in 2D radiographs. Some may also be hemispherical or truncated spheres if touching or attached to the crucible. We used an automated technique for multiple-circle detection in 2D radiographs, based on the Circular Hough Transform (CHT) [24] to determine bubble radius. This CHT-based approach employs a Sobel edge detector [25] to highlight sharp changes in intensity and a thinning algorithm [26] to repeatedly remove pixels from the edges of circular objects until they are reduced to single-pixel-wide shapes (i.e. topological skeletonisation). This image processing pipeline was integrated into the ImageJ software package [27].

3. Results and discussion

3.1. Time-resolved radiographs

Fig. 2(a)–(d) show a series of radiographs collected via *in situ* synchrotron radiation X-ray imaging while an Al–10 wt% Cu alloy melt was subjected to an imposed ultrasound field. Note that Fig. 2 presents a local region from the bottom part of the field of view (~5–6 mm away from the sonotrode tip) where bubbles were minimally disturbed by the cavitation zone in our observation. The gas (bubble interior) and the alloy have very different X-ray attenuation coefficients; this produced good contrast which enabled us to identify bubbles easily. The sonicator pulse sequence is shown in Fig. 2(g). Fig. 2(e) and (f) were generated by subtracting (b) from (a) and (c) from (b), respectively.

Fig. 2(a), (b) and (c) represent the typical appearance of cavitation bubbles in the presence of an ultrasound field during one cycle (1000 ms). Fig. 2(a) shows the cavitation bubbles generated in the ultrasound field shortly after the start of sonication (78 ms). Fig. 2 (b) suggests that the ultrasonication enables a steady growth of cavitation bubbles before it stops at 500 ms. When a new cycle starts, existing bubbles disappear and new cavitation bubbles are formed, as shown in Fig. 2(d). It is also apparent that the majority of bubbles grow slightly in size within our observation capacity. The growth of bubbles can be observed more clearly by detecting the movements of bubble edges and/or the changes in relative distances between bubbles, since bubbles in this region are less disturbed by the liquid flow induced by the sonotrode. As a qualitative example directly appearing in the images, the growth in radius of bubbles indexed with 'A' and 'B' in Fig. 2 can be noticed clearly in their magnified images, as shown by Fig. 2(a.A), 2(b.A), 2 (c.A) and Fig. 2(a.B), 2(b.B), 2(c.B), respectively. Additionally, the edges of the two closely positioned bubbles in the dashed box in Fig. 2(a) overlap (in the 2D radiography images) in its sequential images in Fig. 2(b) and (c), indicating the growth and/or movement of bubbles with time. It is measured that the radii of bubbles marked with 'A', 'B' and 'C' in Fig. 2 are increased from 32 ± 1 μm to 44 ± 1 μm, from 81 ± 1 μm to 97 ± 1 μm, and from 101 ± 1 μm to 118 ± 1 μm as the time is progresses from 78 ms to 1000 ms (i.e. the end of the cycle), respectively. This suggests a fast initial growth within a very short time (from the beginning of a cycle to ~78 ms) followed by relatively slower growth during the rest of the cycle (from 78 ms to the end of a cycle).

By subtracting image (b) from image (a), the bubble evolution under sonicating conditions can be determined. As can be seen from the difference image in Fig. 2(e), i.e. from the crescent shapes on one side of cavitation bubbles (indicated by solid white arrows), the majority of bubbles increased in size, while the centre of most bubbles shifted slightly downwards. This downward motion is assumed to be caused by pressure wave of the sonication source, which is located above and out of the image.